Surface gravity-wave lensing

Ryan B. Elandt, Mostafa Shakeri, and Mohammad-Reza Alam*
Department of Mechanical Engineering, University of California, Berkeley, California 94720, USA
(Received 14 September 2013; published 19 February 2014)

Here we show that a nonlinear resonance between oceanic surface waves caused by small seabed features (the so-called Bragg resonance) can be utilized to create the equivalent of lenses and curved mirrors for surface gravity waves. Such gravity wave lenses, which are merely small changes to the seafloor topography and therefore are surface noninvasive, can focus or defocus the energy of incident waves toward or away from any desired focal point. We further show that for a broadband incident wave spectrum (i.e., a wave group composed of a multitude of different-frequency waves), a polychromatic topography (occupying no more than the area required for a monochromatic lens) can achieve a broadband lensing effect. Gravity wave lenses can be utilized to create localized high-energy wave zones (e.g., for wave energy harvesting or creating artificial surf zones) as well as to disperse waves in order to create protected areas (e.g., harbors or areas near important offshore facilities). In reverse, lensing of oceanic waves may be caused by natural seabed features and may explain the frequent appearance of very high amplitude waves in certain bodies of water.

DOI: 10.1103/PhysRevE.89.023012 PACS number(s): 47.35.Bb, 42.79.Dj, 92.10.Sx, 91.50.Ga

I. INTRODUCTION

Seafloor irregularities affect overpassing surface gravity waves via a number of linear and nonlinear mechanisms [1]. For instance, weakly nonlinear waves traveling over a randomly rough seabed are damped as a result of seafloor's irregularities dispersing the energy of overpassing waves to all spatial directions and at nearly all wave frequencies [2–4]. (This spatial attenuation is called localization [5] because of its common root with Anderson localization in solid-state physics [6].) If seabed corrugations follow specific patterns (i.e., they are not random) then they can excite a number of resonance phenomena between surface waves (depending on the conditions satisfied [7–12]). Resonance of surface waves via bottom undulations is called Bragg resonance named after its close cousin phenomenon in solid-state physics of crystals [13].

Physically speaking, if a proper Bragg resonance condition is satisfied then a surface wave can excite a new (resonant) surface wave in a new direction different from its own original direction (so-called class I, II), or, two surface waves can excite a new wave with a frequency equal to the sub- or superharmonic of primitive waves (so-called class III). In other words, bottom ripples, under Bragg resonance, act as an energy transfer bridge enabling the energy of the incident wave(s) to flow to a new (i.e., resonant) wave. If the interaction distance is long enough, then the resonant exchange continues until the entire energy of initial wave(s) is conveyed to the resonant wave. In perturbation expansion of the governing equations in terms of a small parameter (usually wave steepness ka, k being the wavenumber and a the amplitude of the wave), Bragg resonance occurs at the second order (class I), third order (class II and III), and higher orders of nonlinearities [7,14].

Here we report a seabed corrugation architecture, designed based on properties of Bragg resonance, that can change the direction of propagation of overpassing surface waves toward (or away from) a specific focal point. The apparent first and most important application of this idea is to converge or diverge initially parallel wave rays. Bottom corrugations can therefore be used to create (surface-noninvasive) curved lenses and mirrors for surface gravity waves similar to how curved lenses and mirrors focus or defocus light beams. We further propose a multichromatic bottom that can focus an incident broadband wave spectrum with a high efficiency.

II. THEORY

Consider an incident surface gravity wave of wavenumber vector $\mathbf{k_i}$ and frequency ω propagating in a homogeneous water of mean depth h. Assume that a finite patch of the seabed contains small amplitude periodic ripples with the wavenumber $\mathbf{k_b}$ (similar to seabed sandbars seen in nearshore areas). Over this patch of bottom undulations, if certain conditions between ripples' geometric properties and the overpassing surface waves are satisfied (the so-called Bragg resonance condition), then a new wave with the wavenumber $\mathbf{k_r}$ and the same frequency as the frequency of the incident wave (ω) will be *resonated* (i.e., generated).

Without loss of generality, we consider that the incident wave $\mathbf{k_i}$ moves along positive x axis. If we draw a circle centered at the origin and with a radius $k_i = |\mathbf{k_i}|$, then any vector drawn from the origin to a point on this circle (say $\mathbf{k_r}$) represents the direction of propagation of a resonant wave *if* bottom ripples wavenumber vector $\mathbf{k_b}$ satisfies the class I Bragg resonance condition, i.e., $\mathbf{k_b} = \mathbf{k_r} - \mathbf{k_i}$ [7,14]. Under this circumstance, the amplitude of the incident wave decreases (exponentially over the patch) and the amplitude of the resonant wave increases in such a way that the energy of the entire system of waves is conserved. Outside of the patch, both incident and resonant waves continue to travel with no further change (Fig. 1). Note that class I Bragg resonance is a triad resonance (between two equifrequency surface waves $\mathbf{k_i}$,$\mathbf{k_r}$ and one bottom component $\mathbf{k_b}$), which is obtained at the second order of nonlinearity in terms of wave steepness. If third-order nonlinearities are taken into account, then quartet resonances are obtained between two equifrequency free waves and two bottom components, or, between three free waves and one bottom component [7]. These higher-order resonances are significantly weaker (than the leading order) and are not considered here.

*Corresponding author: reza.alam@berkeley.edu

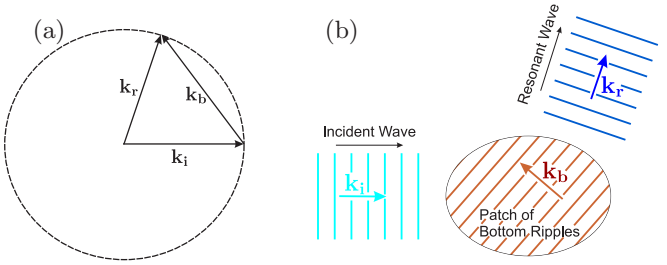

FIG. 1. (Color online) (a) Geometric construction of the class I (triad) Bragg resonant waves. (b) Physical implication of class I Bragg resonance: an incident wave with the wavenumber vector $\mathbf{k_i}$ (assumed to move along the positive x axis) resonates the resonant wave $\mathbf{k_r}$ upon the interaction with the topography with the wavenumber $\mathbf{k_b}$.

Our objective is to design a patch in such a way that the resonant waves formed at each location of the patch are directed toward a desired *focal* point. If this is achieved, high-amplitude motion is expected at the focal point due to the superposition of the arriving resonant waves from all over the patch. Consider a coordinate system in the physical domain with x, y axes on the mean seafloor and z axis positive upward. Assume that a finite two-dimensional patch (in x-y plane) is given across which small ripples can be placed or crafted. The focal point can be at any location on the free surface above or far from the given seabed patch. We specifically consider two cases: the focal point on the upstream and on the downstream side of the patch. In an analogy to optics, we call these configurations, respectively, a *concave mirror* and a *convex lens* of gravity waves [cf. Figs. 2(a)–2(c)].

The design recipe of gravity lenses, based on the theory of Bragg resonance, can be simplified as follows. Consider any arbitrary point in the x-y plane as the focal point. For the ease of notation, assume that the coordinate system (in physical domain) is centered at this focal point. Also, assume that the incident wave is a monochromatic long-crested wave propagating in the positive x direction. To achieve focusing at the focal point, at any point (x, y), the resonant wave wavenumber vector $\mathbf{k}_r$ must be toward the origin $(x, y) = (0,0)$. Therefore, $\mathbf{k}_r$ has to make an angle $\theta = \tan^{-1}(y/x)$ with the negative x axis. Therefore,

$$k_{bx} = k_i(1 + \cos\theta), \quad k_{by} = k_i \sin\theta. \tag{1}$$

Note that, since bottom topography is stationary, if the direction of the bottom wavenumber changes by $\pm\pi$ radians, the same result is obtained.

Physically speaking, Eq. (1) says that the bottom wavenumber vector (i.e., both the wavelength and the direction of ripples) at any location (x, y) of the patch must be different from neighboring points. In order to design a patch, that focuses wave rays toward a focal point, an approximate but handy approach is to divide the patch into a finite number of smaller subpatches. Then each subpatch is covered with uniform ripples with the wavenumber equal to the mean wavenumber of the subpatch required for focusing, say the wavenumber at the center of that specific subpatch [cf. Fig. 1(b)]. This approach proves to work if subpatches are relatively large compared to wavenumber of the incident wave. However, the focal point is not very sharp and discontinuities

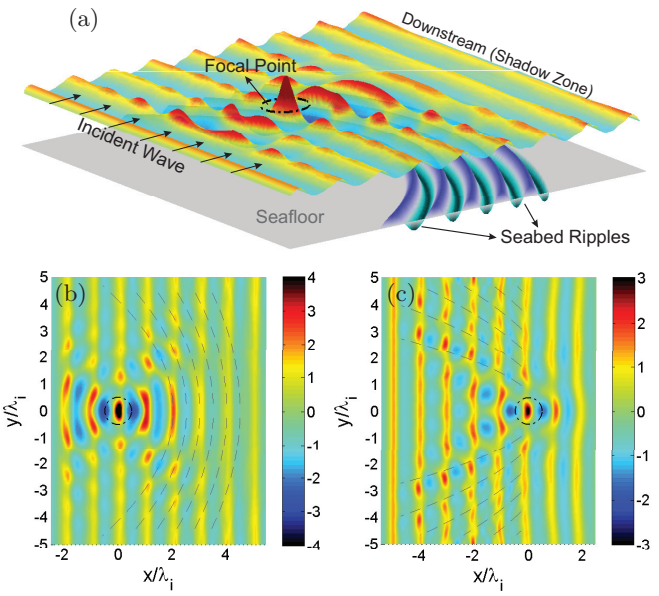

FIG. 2. (Color) (a) Schematic representation of the gravity wave lensing: Incident waves enter from left and upon resonance interaction with the (properly designed) seabed ripples get focused at a desirable focal point. The focal point can be designed to be on the upstream as well as the downstream side of the patch. In analogy to optics, we call these configurations, respectively, a *concave mirror* and a *convex lens*. (b) Direct simulation of a concave mirror for gravity waves. In this case, a monochromatic surface wave of $\epsilon_i = k_i a_i = 0.080$ and $k_i h = 0.84$ enters from left and upon interaction with the rippled patch (maximum of $\epsilon_b = k_b a_b = 0.640$) its energy gets focused at the designated focal point at $x/\lambda_i = 0$ (λ_i is the wavelength of the incident wave). In the snapshot shown ($t/T_i = 14.7$, T_i is the period of the incident wave), at the focal point η_f/a_i=6.3, i.e., surface elevation at the focal point is 6.3 times the amplitude of the incident wave. Simulation parameters are $Nx = Ny = 256$, $\delta t/T_i = 30$, and $M = 3$ for which the simulation is converged. (c) Direct simulation of a convex lens for gravity waves. Parameters are the same as in panel (b) except $\epsilon_{b,\max} = 0.450$. For the snapshot shown ($t/T_i = 9.6$), $\eta_f/a_i = 2.7$. In both cases, the amplification factor increases by the increase in the amplitude and number of ripples.

at the edges of adjacent subpatches cause unwanted scattering and instabilities in overpassing waves.

Here we present a methodology that obtains the continuous geometry of ripples for the entire patch in order to achieve an exact focusing. First, note that the bottom wavenumber $\mathbf{k}_b = \mathbf{k}_b(x, y)$ at each point is perpendicular to the crests and troughs of the bottom undulations, but both the direction and magnitude of $\mathbf{k}_b$ is variable over the patch. The objective is to find a continuous topography whose local wavenumber at each location on the patch satisfies Eq. (1). To achieve this, we define the vector $\mathbf{n}_b$ perpendicular to $\mathbf{k}_b$ (and hence along the wave crests) with the magnitude equal to the magnitude of the $\mathbf{k}_b$ at that location, that is,

$$n_{bx} = -k_i \sin\theta, \quad n_{by} = k_i(1 + \cos\theta). \tag{2}$$

It then can be shown readily that

$$\frac{\partial n_{bx}}{\partial x} + \frac{\partial n_{by}}{\partial y} = 0, \tag{3}$$

that is, $\mathbf{n}_b = (n_{bx}, n_{by})$ form a pseudovelocity field that satisfies continuity. Therefore, a continuous stream-function can be defined for the vector field $\mathbf{n}_b$. Since $\mathbf{k}_b$ is perpendicular to the streamlines of the vector field $\mathbf{n}_b$, these streamlines give the same-height contours of the topography (including, e.g., crests and troughs). As a result, once the ripple's height is specified, the three-dimensional topography can be uniquely obtained. These streamlines are shown by dashed-lines (one wavelength apart) in Figs. 2(b) and 2(c) and the actual topography is shown in Fig. 2(a).

It is to be noted that if the steepness of seabed corrugations are small and of the same order of magnitude as of surface waves (which is the case in the present paper), then the effect of bottom corrugations first appears at the second order of nonlinearity (cf. Refs. [7,14]) and therefore the interaction is nonlinear. Also, since the spatial variation of the bottom is fast (same order as the overpassing surface waves), then the ray theory in its original form does not apply. But a modified ray theory with bottom as quasilinear terms may be used to find the location and the approximate strength of the focusing.

III. DIRECT SIMULATION

To show the performance of the gravity wave lensing, we use a high-order pseudospectral direct simulation technique to numerically solve the governing equation (Laplace's equation) along with the associated (nonlinear) boundary conditions [7,14,15]. This scheme is a phase-resolved direct simulation tool that takes into account the evolution and simultaneous interaction of many [typically $N = O(10^4)$] number of waves with an arbitrary order of nonlinearity [typically $M = O(10)$ in terms of perturbation expansion]. It has been extensively investigated for convergence and cross-validation against analytical and experimental results in different setups [7,14,16–19]. Direct simulation is used here to, besides validating our theoretical predictions, study in detail the nonlinear problem of monochromatic and broadband surface waves impinging upon gravity wave lenses and mirrors.

We first study the problem of a monochromatic wave train incidence on a concave mirror [Figs. 2(a) and 2(b)]. Consider an incident wave of steepness $\epsilon_i = k_i a_i = 0.080$, where k_i, a_i are, respectively, the wavenumber and amplitude of the incident wave, arriving from $-\infty$ and moving along the positive x axis in an open ocean of normalized water depth $k_i h = 0.84$. We set the focal point to be at $(x_f, y_f) = (0,0)$ and choose to have five ripples extending across the seabed. Location of ripples are chosen downstream of the focal point and we decide they start within the area $2\lambda_i < x < 4.5\lambda_i$ along the centerline and extend in $\pm y$ directions ($\lambda_i = |\mathbf{k_i}|/2\pi$ is the wavelength of the incident wave). If more ripples are used, stronger focusing is obtained until the strength is so large that higher-order nonlinearities start to intervene. The area that each single ripple occupies on the seafloor is shown by dashed lines in Fig. 2(b). As shown in the figure, wavenumber of ripples change and they bend as we move away from the $y = 0$ axis (the ripples shape just like a desktop concave mirror). Maximum bottom steepness is along the centerline and is equal to $\epsilon_b = k_b a_b = 0.64$.

We perform a high-order nonlinear direct simulation of the above case in the computational domain. Simulation parameters are $Nx = Ny = 256$, $\delta t/T_i = 30$, and $M = 3$, for which the simulation is converged. Note that class I Bragg resonance is a second-order phenomenon and therefore technically a second-order analysis (i.e., $M = 2$) is enough to capture this effect. Since our spectral method is based on Fourier expansion, the horizontal boundaries are periodic in both x, y directions. We choose a simulation domain larger than the domain of interest and also implement a numerical absorbing beach on the outgoing side of the domain.

Figure 2(b) shows a snapshot of the water surface after a steady-state condition is reached. The specified focal point area is shown by a dashed-line circle where the amplitude grows to more than six times the amplitude of incident wave. A similar case with the focal point on the downstream side of the topography (a convex lens) is shown in Fig. 2(c). In this case, we choose $\epsilon_b = k_b a_b = 0.45$ and arrive at the amplification factor of 2.7 at the focal point. The amplification factor increases by the increase in the amplitude of the topography as well as the increase in the area of the seabed patch.

Analytical expression for the amplification factor at the focal point is not readily at hand; however, an approximation of the focal amplitude height may be obtained. The two-dimensional problem of Bragg resonance of monochromatic waves over a rippled bottom can be solved via perturbation techniques. The reflection coefficient, R, defined as the amplitude of reflected wave divided by the amplitude of incident wave is given by

$$R(x, \mathbf{k}, \mathbf{k_r}) = \frac{g d (\mathbf{k} \cdot \mathbf{k_r}) x}{4 C_{\mathrm{gr}} \omega \cosh kh \cosh k_r h}, \tag{4}$$

where d is the amplitude of the bottom topography, h is the water depth, C_{gr} is the group velocity of the resonant wave, x is the distance of interaction, and g is the gravity acceleration [14]. The reflection coefficient R defined in Eq. (4) is for the two-dimensional ripples, i.e., when ripples are infinitely long in the transverse direction extending to $\pm\infty$. For a finite-width patch (i.e., finite in the transverse direction) no closed-form solution exists [12]. A rough leading-order approximation, hinted by results of Ref. [12], is that the reflection coefficient can be approximated by $R^* = R\ \delta y/(2\lambda_i)$ where δy is the width of the patch and is assumed to be much smaller than λ_i. Now the amplitude at the focal point can be found as a summation over the wave reflections from every piece of the patch. In the limit the expression is

$$S_{\max} = 1 + \int_{y_0}^{y_f} \int_{x_0(y)}^{x_f(y)} \frac{1}{2\lambda_i x} R(x, \mathbf{k}, \mathbf{k_r})\, dx\, dy, \tag{5}$$

where $S_{\max}$ is the ratio of the maximum amplitude at the focal point to the amplitude of the incident wave, y_0, y_f coordinates of transverse lines limiting the topography, and $x_0(y), x_f(y)$ are initial and end x coordinates of bottom ripples corresponding to each y. The first term on the right-hand side of Eq. (5) accounts for the incident wave and the second term (integral term) accounts for all the reflections from the gravity wave lens. For the case of Fig. 2(b) (Concave mirror), we obtain $S_{\max} = 5.6$, which has $\sim$10% error compared to the numerically obtained value of 6.3.

A more thorough analysis of multiple scales reveals that the reflection coefficient Eq. (4) does not increase indefinitely

with the increase with x (which is clearly a violation of energy conservation), but over longer patches behaves like $R \propto \tanh(x)$. Therefore, the reflection coefficient asymptotically reaches unity when the longitudinal extend of the patch approaches infinity. In other words, the strength of the focusing increases with the increase in the number of ripples, but the rate of growth of strength becomes exponentially slow as the number of ripples becomes very large.

Bragg resonance and the resulting focusing phenomenon are also achieved if there is a small detuning between the wavenumber of the incident waves and those of the bottom required to achieve a perfect resonance. The strength of the focusing, however, decreases as the detuning increases until detuning is large enough and focusing disappears (cf., e.g., Fig. 5 in Ref. [17], which is an example of how detuning affects the strength of Bragg resonance).

IV. EXPERIMENT

We also present an experimental proof of the gravity wave lensing. We consider a case of $k_i a_i = 0.157$, $k_i h = 1.57$ and a maximum of $k_b a_b = 1.26$. In a physical wave tank of the size of 60 m × 2.4 m (width) × 1.8 m (depth), these correspond to the mean water depth of 15 cm, incident wave amplitude and wavelength of, respectively, 1.5 mm and 60 cm, topography wavelength along the centerline 30 cm, and topography amplitude of 6 cm. A rigid 2.4 m × 2.4 m three-dimensional topography was constructed by first placing 12 CNC-machined wooden guides along the longitudinal direction. The guides were covered with plastic chicken wire, a fiberglass mat, and fiberglass resin. The hardened fiberglass was sanded to achieve the required smoothness. A view of the middle section of the wave tank is shown in Fig. 3(a) with crests of the topography visible through the water [also cf. Fig. 3(b)].

Laser-induced fluorescence (LIF) was used to record the wave surface profile histories at 20 sections parallel to the wave tank wall. Specifically, two 1-Watt continuous wave lasers were used to create vertically oriented laser sheets in order to illuminate the surface of the wave. The lasers were mounted 60 cm apart on aluminum profiles and connected to a track with increments marked every 6 cm. The lasers excited the fluorescent dye Fluorescein. Fluorescein has a peak absorption at 494 nm and a peak emission at 521 nm. Videos of the water surface were recorded with a digital camera at 15 fps. The camera was positioned inside the wave tank and above the free surface. Videos were taken of the surface starting in the middle plane and going to the plane 114 cm away from the centerplane. The videos were converted into individual images and the images were analyzed in MATLAB. Canny edge detection was used to determine the intersection of the laser sheet and the water free-surface in each image.

A side-by-side comparison of the experiment and the numerical simulation is shown in Fig. 3(c), where good agreement is observed (for a full video see Supplemental Material [20]). The maximum amplitude at the focal point [marked with white dashed-lines in Fig. 3(c)] is about three times the amplitude of the incident wave.

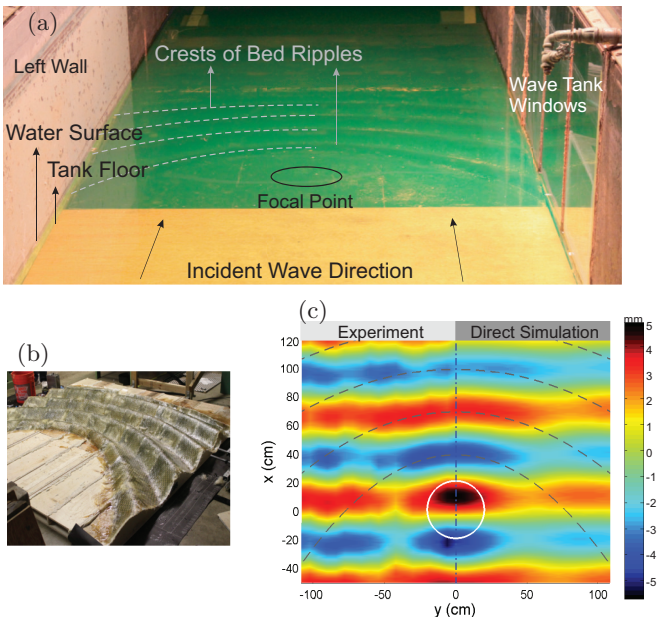

FIG. 3. (Color) Experimental investigation of the gravity wave lensing. (a) Experimental setup. The photograph shows the middle section of a 60 m × 2.4 m (width) × 1.8 m tank at the U.C. Berkeley's Richmond Field Station. To measure the time evolution of the water surface profile, a laser-induced fluorescence (LIF) technique was used (greenish color is due to fluorescent dye). Ripple crests [cf. panel (c)] can be seen through the water and are marked by dashed lines on the left side of the figure. (b) The 2.4 m × 2.4 m rippled patch before it is colored in black and placed inside the wave tank. (c) A side-by-side comparison of the experimental (left) and direct simulation (right) results. The experiment is designed for a monochromatic incident wave of $\epsilon_i = 0.016$, $k_i h = 1.57$, and $\epsilon_{b,\max} = 1.26$. In terms of physical variables, these parameters correspond to a water depth of 15 cm, incident wave amplitude of 1.5 mm, and wavelength of 60 cm, topography wavelength along the centerline of 30 cm, and topography amplitude of 6 cm (see Supplemental Material movies 1 and 2 in Ref. [20]).

V. BROADBAND LENSING

With the theoretical, computational, and experimental proof of the gravity wave lensing for a monochromatic incident wave in hand, the next immediate question is whether the lensing can be achieved in real ocean scenarios where an incident wave group contains a spectrum of frequencies and is composed of a multitude of (linearly or nonlinearly) superposed wave components. Here, we show that broadband lensing is possible through a similar mechanism. For a polychromatic incident wave train, leading-order lensing is achieved by the superposition of proper bottom undulations, each corresponding to one subgroup of incident wave components that have close wavelengths. This, usually, does not require more space than before, but just a polychromatic bottom undulation, hence can be readily achieved. The efficiency of broadband lensing by this method is shown here through a case study via direct simulation.

Consider a Gaussian spectrum with a normalized spectral density function $S^*(\omega_r) = 0.65\exp[-21(\omega_r - 1)^2]$, where $\int S^* \mathrm{d}\omega_r = \sum_j 1/2(a_j/a_s)^2$, in which $\omega_r = \omega/\omega_p$, ω_p is the

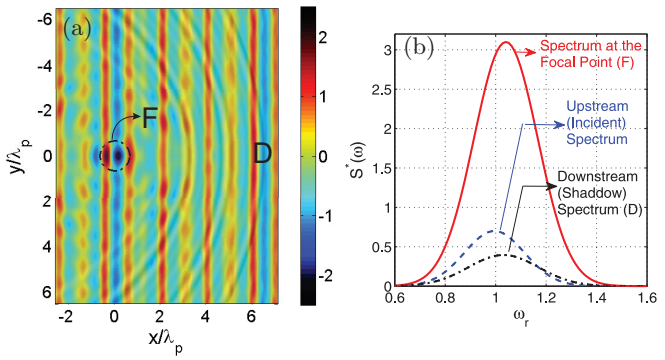

FIG. 4. (Color) Gravity wave lensing for a broadband incident spectrum. To achieve focusing in this case, the topography needs to be polychromatic. (a) A water-surface snapshot from direct simulation of focusing of a broadband (Gaussian) incident spectrum. Colors show the surface elevation normalized by the significant wave amplitude ($a_s = H_s/2$, where H_s is the significant wave height). In the snapshot shown, the waveheight of the wave seen at the focal point exceeds $4a_s = 2H_s$ and therefore is a rogue wave by definition. (b) Steady-state spectra at the upstream (blue dashed line) and downstream (black dash-dotted line) of the lensing area compared with that at the focal point (red solid line). Clearly, the spectrum at the focal point (F) has a much higher energy (about four times the energy of the incident spectrum). The downstream (shadow zone) spectrum, as expected, has a lower level of energy. In this figure, ω_p is the peak frequency of the spectrum, and normalized spectral density function $S^*(\omega)$ is defined as $\int S^* d\omega = \sum_j 1/2(a_j/a_s)^2$. Simulation parameters are $Nx = Ny = 512$, $\delta t/T_p = 30$, and $M = 4$, for which the simulation is converged.

peak frequency, and a_s is the significant wave amplitude (i.e., $a_s = H_s/2$, where H_s is the significant wave height). For a direct phase-resolved simulation, we assume that the surface is composed of seven waves at frequencies $\omega_r = 0.67$, 0.80, 0.93, 1.05, 1.15, 1.24, and 1.33. We design three separate topographies corresponding to every other wave of this list, i.e., for surface wave frequencies $\omega_r = 0.80$, 1.05, and 1.24. We further assume that a specific area is provided for ripples and therefore for the three topographies, respectively, 7, 10, and 13 ripples can be placed on this area. We then superimpose these three structures. Contours of the topography in darker and brighter bands are superimposed to Fig. 4(a).

Results of the direct simulation of the broadband spectrum incident to this patch is shown in Figs. 4(a) and 4(b). Figure 4(a) shows a surface snapshot at $t/T_p = 95$ ($T_p = 2\pi/\omega_p$), where a strong wave focusing is observed at the focal point. At this moment, the wave height at the focal point (H_f) is greater than four times the significant wave amplitude and therefore by definition is a rogue wave at this sea state ($H_f = 2.19\, H_s$). Long-term spectrum of the incident wave, the spectrum at the focal point, and downstream of the lens are compared in Fig. 4(b). Spectrum at the focal point is much more energetic than the incident wave and reaches an amplitude more than four times higher. As expected, the downstream spectrum has less energy than the incident spectrum.

Theoretical analysis, tracing of waves, and interpretation of the details of the results in broadband lensing is more complicated than those of monochromatic lensing. Usually when more than just a few wave components simultaneously present on the water, a complex network of interwoven nonlinear interactions forms. Inclusion of a polychromatic bottom topography further complicates the scenario. These interactions include, for instance, sub- and superharmonic generations [21–23], quartet resonance between waves [24,25], and higher-order Bragg resonances [7,14]. The direct simulation scheme of higher-order spectral method used to simulate the above cases efficiently takes all these interactions into account [17,19].

Gravity wave lensing can, theoretically, be achieved at any water depth and for any amplitude of ripples. The efficiency of lensing increases linearly with both the number and amplitude of ripples and decreases exponentially with the increase in the water depth. This means that, to achieve the same efficiency in a deeper water, a much higher number of ripples are needed and/or ripples must have much higher amplitude. Monochromatic convex focusing can also be achieved using refraction properties of water waves [26–28]. Refraction-based focusing, however, only works for monochromatic waves, requires a relatively large flat plate submerged but kept stationary close to the water surface, and has a low-efficiency due to unwanted yet unavoidable reflection of the incident wave [29].

Gravity wave lensing provides a powerful tool for manipulating ocean waves. The efficiency of the idea is particularly significant over the shallower areas of the ocean such as continental shelves. Wave lensing may substantially contribute to the efficiency of ocean wave energy devices by providing localized high-energy wave zones. Therefore, instead of a large number of (small and low-efficiency) wave energy devices dispersed over a wide area, one (relatively large and high-efficiency) device can be placed at the focal point, receiving the majority of the energy of the initial area. This should be of interest to the environment and also the sea transportation as the covered surface of the sea is significantly reduced. Through the dispersion of wave rays, wave lensing may also have applications in creating localized safe havens for fishermen and sailors in open seas, or if implemented in large scales to protect shores and harbors against strong storm waves. Artificial surf zones, quiet beaches, and open-sea water parks are other potential applications of gravity wave lensing. The lensing of ocean waves may also happen by natural seabed features, and therefore further care must be taken into account for the proper placement of (nearshore) facilities, particularly in the areas with substantial bottom variations.

Bragg scattering, although different in details, is a common concept in solid-state physics [30–32], optics [33], acoustics [34,35], and hydrodynamics [7,11,14]. The idea demonstrated here may have similar implications in any system admitting Bragg resonance and if its medium can be freely architected.

ACKNOWLEDGMENTS

We thank L. A. Couston, S. Demooei, R. Ghosh, M. Lehmann, Y. Liang, Y. Fu, C. Funke, D. Lee, and staff at the U.C. Berkeley Machine Shop for their help in setting up the experiment. M.R.A. thanks Professor Dick K. P. Yue and Dr. Yuming Liu at MIT, where many aspects of the theory of Bragg resonance were developed under their guidance. The support from the American Bureau of Shipping and U.C. Berkeley's Committee on Research is gratefully acknowledged.

[1] M. W. Dingemans, *Water Wave Propagation Over Uneven Bottoms* (World Scientific, Singapore, 1997).
[2] M. Belzons, E. Guazzelli, and O. Parodi, J. Fluid Mech. **186**, 539 (1988).
[3] M.-R. Alam and C. C. Mei, J. Fluid Mech. **587**, 73 (2007).
[4] M.-R. Alam and C. C. Mei, J. Fluid Mech. **616**, 397 (2008).
[5] P. Devillard, F. Dunlop, and B. Souillard, J. Fluid Mech. **186**, 521 (1988).
[6] P. Anderson, Phys. Rev. **109**, 1492 (1958).
[7] M.-R. Alam, Y. Liu, and D. K. P. Yue, J. Fluid Mech. **643**, 437 (2010).
[8] S. Elgar, B. Raubenheimer, and T. H. C. Herbers, Geophys. Res. Lett. **30**, 1016 (2003).
[9] A. D. Heathershaw, Nature **296**, 343 (1982).
[10] A. G. Davies, Dynam. Atmospheres Oceans **6**, 207 (1982).
[11] C. C. Mei, J. Fluid Mech. **152**, 315 (1985).
[12] J. T. Kirby, J. Fluid Mech. **162**, 171 (1986).
[13] W. H. Bragg and W. L. Bragg, Proc. R. Soc. A **88**, 428 (1913).
[14] Y. Liu and D. K. P. Yue, J. Fluid Mech. **356**, 297 (1998).
[15] D. G. Dommermuth and D. K. P. Yue, J. Fluid Mech. **184**, 267 (1987).
[16] M.-R. Alam, Y. Liu, and D. K. P. Yue, J. Fluid Mech. **624**, 225 (2009).
[17] M.-R. Alam, Y. Liu, and D. K. P. Yue, J. Fluid Mech. **624**, 191 (2009).
[18] M.-R. Alam, Proc. R. Soc. A **468**, 3153 (2012).
[19] M.-R. Alam, Phys. Rev. Lett. **108**, 084502 (2012).
[20] See Supplemental Material at http://link.aps.org/supplemental/10.1103/PhysRevE.89.023012 for videos of the simulations and experimental results.
[21] P. J. Bryant, J. Fluid Mech. **59**, 625 (1973).
[22] C. Mei and U. Unluata, in *Waves on Beaches and Resulting Sediment Transport: Proceedings of an Advanced Seminar Conducted by the Mathematics Research Center, the University of Wisconsin, and the Coastal Engineering Research Center, US Army, at Madison* (Academic Press, San Diego, 1971), p. 181.
[23] M.-R. Alam, Y. Liu, and D. K. P. Yue, J. Fluid Mech. **689**, 529 (2011).
[24] O. M. Phillips, J. Fluid Mech. **9**, 193 (1960).
[25] A. D. D. Craik, *Contemporary Physics*, Cambridge Monographs on Mechanics and Applied Mathematics, Vol. 28 (Cambridge University Press, Cambridge, 1988), pp. xii, 322.
[26] E. Mehlum and J. Stamnes, Proc. of First Symposium Wave Energy Utilization (1979).
[27] J. J. Stamnes, *Waves in Focal Regions: Propagation, Diffraction, and Focusing of Light, Sound, and Water Waves* (Adam Hilger, Briston, UK, 1986), p. 600.
[28] L. Griffiths and R. Porter, Appl. Ocean Res. **34**, 150 (2012).
[29] M. McIver, J. Eng. Math. **19**, 297 (1985).
[30] P. J. Martin, B. G. Oldaker, A. H. Miklich, and D. E. Pritchard, Phys. Rev. Lett. **60**, 515 (1988).
[31] J. Phillips, J. Bean, B. Wilson, and A. Ourmazd, Nature **325**, 121 (1987).
[32] E. Fermi and L. Marshall, Phys. Rev. **71**, 666 (1947).
[33] G. Kryuchkyan and K. Hatsagortsyan, Phys. Rev. Lett. **107**, 053604 (2011).
[34] L. Feng, X.-P. Liu, M.-H. Lu, Y.-B. Chen, Y.-F. Chen, Y.-W. Mao, J. Zi, Y.-Y. Zhu, S.-N. Zhu, and N.-B. Ming, Phys. Rev. Lett. **96**, 014301 (2006).
[35] D. Nicholas and C. Hill, Nature **257**, 305 (1975).